Developmental Cell, Vol. 6, 371–382, March, 2004, Copyright ©2004 by Cell Press

Fibronectin Regulates Epithelial Organization during Myocardial Migration in Zebrafish

Le A. Trinh and Didier Y.R. Stainier*
Department of Biochemistry and Biophysics
Programs in Developmental Biology, Genetics and Human Genetics
University of California, San Francisco
San Francisco, California 94143

Summary

Several genes have been implicated in heart tube formation, yet we know little about underlying cellular mechanisms. We analyzed the cellular architecture of the migrating myocardial precursors, and find that they form coherent epithelia that mature as they move medially. Mutant analyses indicate that the cardia bifida locus *natter* (*nat*) is required for the integrity of the myocardial epithelia. We positionally cloned *nat* and show that it encodes Fibronectin. During myocardial migration, Fibronectin is deposited at the midline between the endoderm and endocardial precursors, and laterally around the myocardial precursors. Further analyses show that Fibronectin deposition at the midline is required for the timely migration of myocardial precursors, but dispensable for the migration process itself. In the complete absence of Fibronectin, adherens junctions between myocardial precursors do not form properly, suggesting that cell-substratum interactions are required for epithelial organization. These data suggest that myocardial migration is dependent on epithelial integrity.

Introduction

In all vertebrates, the heart tube, which consists of a myocardial and an endocardial layer, develops from bilateral populations of cells in the anterior lateral plate mesoderm (LPM) (reviewed by McFadden and Olson, 2002). During somitogenesis, the myocardial precursors appear to move coordinately toward the midline in concert with the anterior LPM, and fuse to form the outer, muscular layer of the heart tube. Large-scale genetic screens in zebrafish have identified mutations in eight loci that disrupt this process, resulting in the formation of two separate hearts, a phenotype referred to as cardia bifida (Chen et al., 1996; Stainier et al., 1996; Alexander et al., 1998). Analyses of these mutants have led to the identification of several requirements for myocardial migration. First, myocardial differentiation appears to be critical for migration as mutants with defective myocardial differentiation exhibit migration defects (Reiter et al., 1999, 2001; Yelon et al., 2000). Second, an interplay between the myocardial precursors and the endoderm is thought to be essential for heart tube formation, as mutants that lack the anterior endoderm display cardia bifida (Schier et al., 1997; Alexander et al., 1999; Reiter et al., 1999; Kikuchi et al., 2000). Additionally, chimera and cell transplantation analyses in mouse and zebrafish indicate that wild-type endoderm can rescue the myocardial migration defects in a subclass of cardia bifida mutants (Narita et al., 1997; David and Rosa, 2001). Though these studies point to an essential role for the endoderm in myocardial migration, it is unclear whether it is providing a substrate or signal for migration.

In chick embryos, one substrate at the interface between the endoderm and mesoderm implicated in myocardial migration is Fibronectin (Fn). Fn, a major constituent of the extracellular matrix (ECM), mediates a wide range of cellular processes through its interaction with the Integrin receptor family to promote cell-substratum adhesion and spreading, cell migration, cell cycle progression, and cytoskeletal organization (reviewed by Hynes, 1992; Sechler and Schwarzbauer, 1998; Danen and Yamada, 2001). It has been further reported that in chick embryos Fn is deposited in an anterior-to-posterior gradient between the endoderm and mesoderm during myocardial migration (Linask and Lash, 1986). Additionally, treatment of chick embryos with an antibody against Fn arrests heart tube formation (Linask and Lash, 1988). From these observations, it has been proposed that a gradient of Fn provides the directional cue for myocardial migration (Linask and Lash, 1988). However, other studies have been unable to replicate these observations, and reported either a uniform or anteriorly localized distribution of Fn in the heart-forming region of chick embryos (Drake et al., 1990; Wiens, 1996). Therefore, while it is clear that in chick embryos Fn is deposited at the interface between the endoderm and mesoderm, its precise distribution and the mechanisms by which Fn might regulate myocardial migration remain to be defined.

Fn also appears to be required for myocardial migration in mice. Mouse embryos deficient for Fn die around E8.0–8.5 with defects in the neural tube, vasculature, notochord, somites, and heart (George et al., 1993). Analyses of the heart defect in the Fn null embryos indicate that myocardial specification occurs normally but that myocardial migration is defective (George et al., 1997). Thus, while these studies clearly show a requirement for Fn in myocardial migration, the cellular basis of this requirement is unclear.

Although multiple mouse and zebrafish loci regulate myocardial migration, we know little about the cellular mechanisms of this process. Myocardial migration has been described to proceed in an organized fashion, but it is unclear whether the myocardial precursors move as a coherent population or as individual cells that are responding to environmental cues. Studies in chick embryos suggest that the migrating myocardial precursors form epithelial sheets as cell junctional proteins such as N-cadherin and catenins show focal localization in the mesodermal cells of the heart-forming region (Linask, 1992; Linask et al., 1997). However, it remains to be determined whether epithelial organization is required for myocardial migration.

We have examined the cellular architecture of the

*Correspondence: didier_stanier@biochem.ucsf.edu

myocardial precursors in zebrafish by confocal microscopy and found that they form polarized epithelia, indicating that they migrate as a coherent population. To better understand the morphogenesis of these epithelia, we have focused on the cardia bifida locus *natter* (*nat*) and show that it encodes Fn. During the stages of myocardial migration, Fn is deposited around the bilateral populations of myocardial precursors as well as at the midline between the endocardial precursors and the overlying endoderm. Analyses in mutant embryos lacking endocardial precursors indicate that Fn deposition at the midline is required for the proper temporal regulation of myocardial migration but is dispensable for the migration process. We further show that Fn deposition is required for proper adherens junction formation, indicating that cell-substratum interactions are essential for maintaining epithelial integrity in the migrating myocardial precursors.

Results

Myocardial Precursors Form Polarized Epithelia during Their Migration to the Midline

To gain a better understanding of the cellular basis of myocardial migration, we used a transgenic line that uses the *cardiac myosin light chain2* (*cmlc2*) promoter to drive green fluorescent protein (GFP) in the myocardial precursors (Huang et al., 2003) in conjunction with various antibodies. Cell boundaries were visualized with an antibody to β-catenin which localizes to the cortex of all cells in the zebrafish embryo (Topczewska et al., 2001). In addition to labeling the cortex, β-catenin antibodies have also been reported to mark adherens junctions (Cox et al., 1996), as well as basolateral domains in polarized epithelia (Piepenhagen and Nelson, 1995). Cell junctions were visualized with an antibody that recognizes atypical protein kinase C λ and ζ (aPKCs). Although aPKCs typically localize to tight junctions in adult epithelia, they localize to adherens junctions in embryonic tissues (Horne-Badovinac et al., 2001; Manabe et al., 2002).

We found that the myocardial precursors form polarized epithelia with distinct localization of junctional proteins during the stages of myocardial migration. At the 16-somite stage, *cmlc2* expression shows that the myocardial precursors are bilateral (Figure 1B) (Yelon et al., 1999). In transverse sections of *cmlc2*::GFP transgenic embryos, the myocardial precursors, labeled by GFP, appear as cuboidal cells outlined by cortical β-catenin (Figures 1C and 1D). The anterior LPM has been described to form bilateral tubular primordia (Stainier et al., 1993). It appears that the myocardial precursors occupy predominantly the ventral side of the LPM tubules, with a few cells positioned dorsally in the medial domain. aPKCs appear to be restricted to the ventricular surface of the neural tube and the myocardial precursors (Figure 1D). In these latter cells, aPKCs are localized along the apical side in a variable, punctate pattern and enriched at points of cell-cell contacts (Figures 1C and 1D). This enrichment of aPKCs at points of cell-cell contacts suggests that the myocardial precursors are forming immature epithelia at the start of myocardial migration to the midline.

As migration proceeds, cell junctional proteins show an increased asymmetric localization in the myocardial precursors. At the 18-somite stage, the posterior myocardial precursors have reached the midline, resulting in a V-shaped pattern of *cmlc2* expression (Figure 1E) (Yelon et al., 1999). In transverse sections, more GFP positive cells are seen on the dorsomedial aspect of the LPM tubules (Figures 1F and 1G). Thus, it appears that at the 18-somite stage the myocardial precursors occupy more of the LPM tubules. Interestingly, β-catenin localization transitions from the cortical localization seen at the 16-somite stage to become asymmetric and restricted to the basolateral domains of the myocardial precursors (Figure 1G). In contrast, aPKCs appear to be localized to the apicolateral domains of the myocardial precursors (Figure 1G).

At the end of myocardial migration, the restricted localization of β-catenin and aPKCs is more prominent, and differences in cell shape can be observed between medial and lateral myocardial precursors. At the 20-somite stage, the myocardial precursors have fused to form the cardiac cone (Figure 1H) (Stainier et al., 1993; Yelon et al., 1999). In transverse sections through the middle of the cardiac cone, the myocardial epithelia have undergone further maturation. The medial cells appear columnar in shape with prominent localization of aPKCs to the apicolateral domain, while the lateral cells have remained cuboidal (Figures 1I and 1J). β-catenin remains excluded from the apical domain and localized to the basolateral domain. The asymmetric localization of aPKCs and β-catenin suggests that during the stages of migration to the midline, the myocardial precursors form maturing polarized epithelia and migrate as coherent populations.

In addition to observing polarized distribution of junctional components in the myocardial precursors, we also observed in the medial-most myocardial precursors changes in cell morphology that suggest these may be leading edge cells. In some transverse sections, the medial-most cells of the migrating bilateral epithelia appear to lose their cuboidal shape and form cellular extensions toward the midline (Figures 1K and 1L). This change in cell morphology and cellular extensions suggest that the myocardial epithelia are undergoing active directional migration.

Morphogenetic and Myocardial Cell Adhesion Defects in *nat* Mutants

To better understand the morphogenesis of the myocardial epithelia, we focused on the *nat* mutation because it appeared to have defects in myocardial migration, as well as myocardial cell adhesion. The *nat* locus was identified in a large-scale screen in Tübingen as a mutation leading to a flattened hindbrain as well as a partially penetrant cardia bifida phenotype (Figure 2B) (Chen et al., 1996; Jiang et al., 1996). Mutations affecting myocardial differentiation can cause cardia bifida (Reiter et al., 1999; Yelon et al., 2000), and thus we wanted to assess myocardial differentiation in *nat* mutants. Based on the expression of *cmlc2*, myocardial differentiation appears unaffected in *nat* mutants. By 24 hours postfertilization (hpf) in wild-type embryos, the two populations of myocardial precursors have fused at the midline to form a

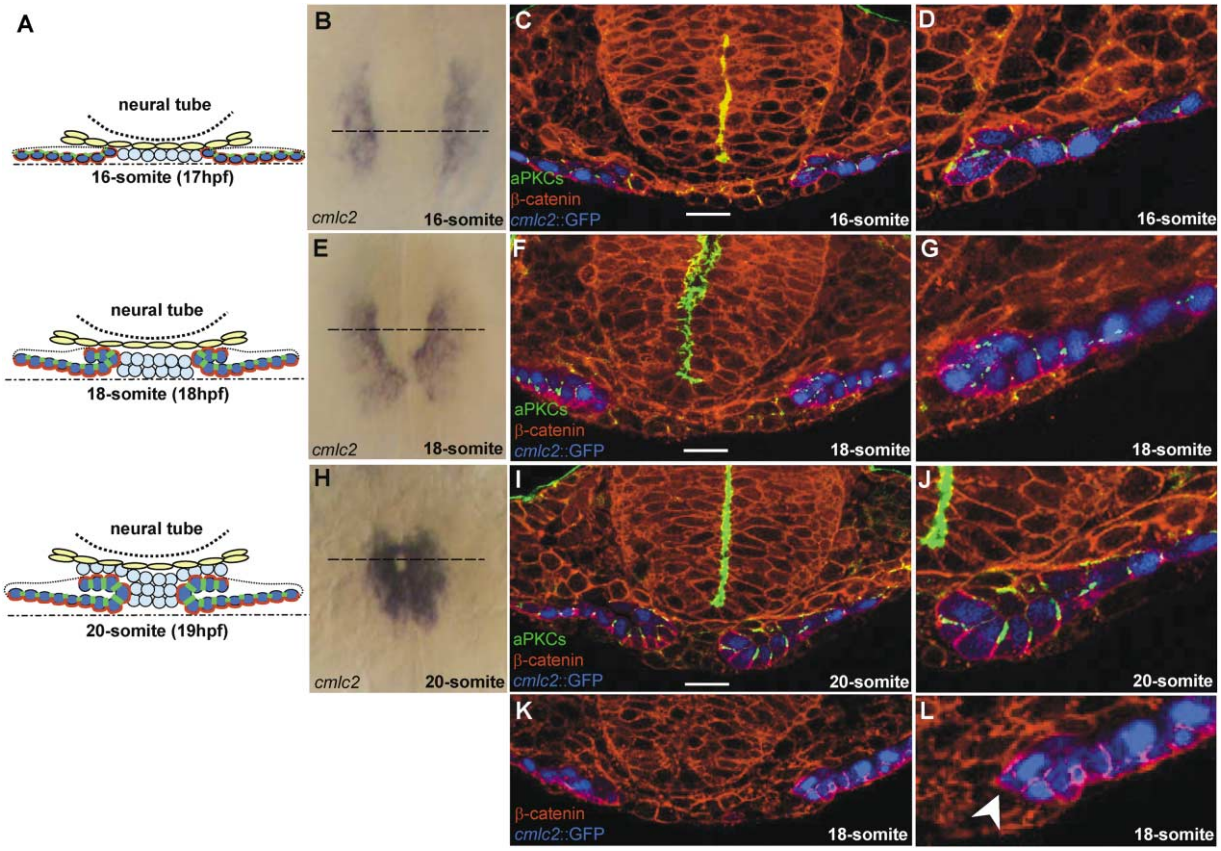

Figure 1. Myocardial Precursors Form Polarized Epithelia during Their Migration to the Midline

(A) Diagrams representing transverse sections of myocardial precursors (dark blue cells) within the LPM tubules (dotted line), endocardial precursors (light blue cells), the overlying endoderm (yellow cells), and the underlying YSL (dashed line), as well as the subcellular localization of cell junctional proteins, β-catenin (red), and aPKCs (green) in the myocardial precursors at the 16-, 18-, and 20-somite stages (17, 18, and 19 hpf).

(B, E, and H) *cmlc2* expression; dorsal views, anterior to the top. Dashed lines indicate the level of the transverse sections in (C), (F), and (I). (C, D, F, G, I, J, K, and L) Transverse confocal images of *cmlc2*::GFP (false colored blue) transgenic embryos immunostained with antibodies against β-catenin (red) and aPKCs (green); dorsal to the top. (K) and (L) were immunostained with antibody against β-catenin (red) only. Scale bars, 20 μm. (D, G, J, L) Magnified view of lower right corner of (C), (F), (I), and (K). (B, C, and D) At the 16-somite stage, the myocardial precursors are bilateral cuboidal cells that line the ventral side of the embryo, and are outlined by cortical β-catenin. aPKCs are localized along the apical side of the myocardial precursors and enriched at points of cell-cell contacts. (E, F, G) At the 18-somite stage, the posterior myocardial precursors have reached the midline (E), and more GFP positive cells are seen in the medial domain of the myocardium (F and G). (G) β-catenin is localized to the basolateral membranes and aPKCs to the apicolateral membranes of the migrating myocardial precursors. (H) At the 20-somite stage, the myocardial precursors have fused to form the cardiac cone. (I and J) In transverse sections through the middle of the cardiac cone, the medial cells appear columnar in shape, while the lateral cells have remained cuboidal. aPKCs staining is more prominent in the medial cells and restricted to the apicolateral membranes, while β-catenin localizes to the basolateral membranes. (K and L) Transverse section at the 18-somite stage: the medial-most cells of the bilateral epithelia appear to lose their cuboidal shape and form cellular extensions toward the midline. (L) Magnified image of (K) shows that the medial-most myocardial cell from the right LPM appears to form a cellular extension toward the midline (arrowhead).

single heart tube (Figure 2C). In *nat* mutants, the myocardial precursors remain as two separate populations at variable distance from the midline (Figures 2D and 2E). Additionally, individual myocardial precursors are seen separate from the main bifid populations in the mutants (Figures 2D and 2E). The separation of *cmlc2* positive cells was first observed in mutants at 22 hpf (data not shown). By this stage, the myocardial precursors have formed polarized epithelia with distinct adherens junctions in wild-type embryos (Figure 1). The presence of individual *cmlc2* positive cells in *nat* mutants suggests that the myocardial precursors may have defects in cell-cell adhesion.

These cardiac morphogenetic defects led us to analyze the morphogenesis of the entire LPM in *nat* mutants. During the stages of myocardial migration, the LPM undergoes a mediolateral expansion as visualized by the two broadening stripes of *dhand* expression (Figure 2F) (Yelon et al., 2000). In *nat* mutants, the mediolateral expansion of the anterior LPM fails to occur and this tissue remains narrow and compact and frequently appears dysmorphic (Figures 2G and 2H). Similar observations were made when we examined *gata4, gata5*, and *hrt* expression (data not shown) (Yelon et al., 2000; Reiter et al., 1999; Griffin et al., 2000). In contrast, the posterior LPM appears unaffected (data not shown). These results

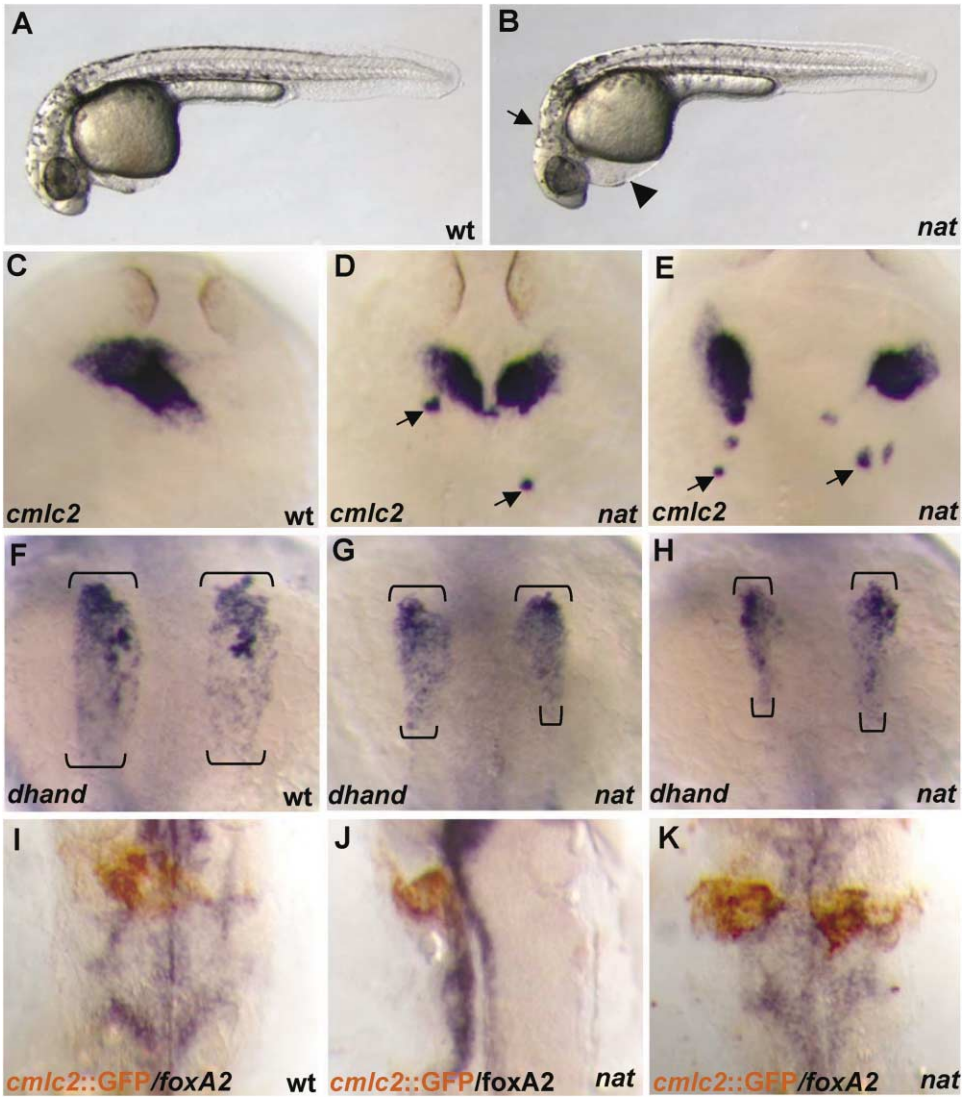

Figure 2. Morphogenetic and Myocardial Cell Adhesion Defects in *nat* Mutants

(A, C, F, and I) Wild-type and (B, D, E, G, H, J, and K) *nat* mutants.

(A and B) Lateral views of brightfield images at 32 hpf, anterior to the left. (B) *nat* mutants display pericardial edema (arrowhead) and a flattened hindbrain (white arrow).

(C–K) Dorsal views of in situ hybridization images, anterior to the top. (C–E) *cmlc2* expression at 24 hpf. (C) Wild-type embryos have formed a single heart tube. (D and E) *nat* mutants have two main populations of myocardial precursors at variable distance from the midline. Additionally, individual myocardial precursors (arrows) are seen detached from the main populations in mutant embryos. (F–H) *dhand* expression in the anterior LPM at the 17-somite (17.5 hpf) stage. Brackets indicate the width of the bilateral anterior LPM stripes. (F) Wild-type embryos show broad stripes of *dhand* expression. (G and H) In *nat* mutants, the bilateral stripes of *dhand* expression are narrower and appear dysmorphic. (I–K) Defects in myocardial and anterior endoderm morphogenesis appear to be independent. Anti-GFP (red) in *cmlc2*::GFP transgenic embryos labels the myocardial precursors, while *foxA2* expression (blue) marks the anterior endodermal sheet. (I) In wild-type embryos at 21 hpf, the anterior endoderm forms a sheet that spreads across the midline, while the cardiac cone is positioned to the left of the midline. (J) In some *nat* mutants, the anterior endodermal sheet fails to extend across the midline, while the myocardial cells have reached the midline. (K) Other *nat* mutants exhibit normal endodermal morphogenesis, while the myocardial precursors have failed to migrate.

indicate that the morphogenetic defects in *nat* mutants expand beyond the myocardial precursors but are restricted to the anterior LPM.

As mutations in genes affecting endoderm formation also exhibit myocardial migration defects (Schier et al., 1997; Alexander et al., 1999; Reiter et al., 1999; Kikuchi et al., 2000), we assessed endoderm formation in *nat* mutants. While specification of endodermal cells is unaffected in *nat* mutants (data not shown), subsequent morphogenesis of the anterior endoderm is sometimes defective. *foxA2* expression marks the anterior endoderm, derivatives of which form the lining of the pharynx (Odenthal and Nüsslein-Volhard, 1998). In wild-type embryos at 21 hpf, the anterior endoderm forms an extended

sheet across the midline with characteristic protrusions along the edges (Figure 2I). In some *nat* mutants, the anterior endodermal sheet undergoes aberrant morphogenesis (Figure 2J). To examine the relationship between the endodermal and myocardial morphogenetic defects in *nat* mutants, we assessed the endoderm (*foxA2*) and the myocardial precursors (anti-GFP in *cmlc2*::GFP transgenic embryos) in parallel by double staining. We observed three classes of mutants: one where both endodermal and myocardial morphogenesis were defective, others where endodermal morphogenesis occurred properly while myocardial migration was defective (Figure 2K), and yet others where endodermal morphogenesis was defective but the myocardial precursors reached the midline (Figure 2J). These data suggest that the endodermal and myocardial morphogenesis defects are independent of one another.

The *nat* Locus Encodes Fn

To gain further insight into the *nat* phenotype, we isolated the gene disrupted by the *nat* mutation. Using bulk segregant analysis (Postlethwait and Talbot, 1997), we mapped the *nat* locus to linkage group 9. Fine mapping with 864 diploid embryos localized *nat* to a region of 2.9 cM between the CA repeat markers z4168 and z99205. Examination of radiation hybrid maps revealed several ESTs in this region, including *fn* (Zhao et al., 2001). Because Fn had been implicated in the morphogenesis of multiple tissues including the precardiac mesoderm (Linask and Lash, 1988; George et al., 1993), we decided to test *fn* as a candidate for *nat*. We developed polymorphisms in the 5′ and 3′ untranslated regions of *fn* and found one and zero recombinant with *nat* in 864 diploid embryos, respectively (Figure 3A). Sequencing of the single *tl43c* allele of *nat* revealed an A to T (AAA→TAA) transversion that introduces a premature translational stop at codon 81 (Figure 3B). To confirm the presence of the A to T transversion at the genomic level, we used a restriction fragment length polymorphism generated by the transversion to genotype *nat* mutants. We found that the transversion segregated with the *nat* phenotype in all embryos examined (n = 243).

To further demonstrate that a defect in *fn* is sufficient to cause myocardial migration defects, we examined the ability of a morpholino antisense oligo (MO) designed against *fn* to phenocopy *nat*. Injection of a *fn* MO into genetically sensitized embryos led to myocardial migration defects as seen by pericardial edema (Figure 3D) and *cmlc2* expression (data not shown). Genetic sensitization was achieved by reducing the maternal contribution of *fn* through the use of heterozygous *nat* females to generate embryos for the antisense-injection experiments. Heterozygous *nat* embryos are phenotypically wild-type. Reduction of maternal gene products through genetic sensitization has been used in morpholino antisense experiments in which high levels of maternal expression have been observed (Walsh and Stainier, 2001). Using genetically sensitized embryos, we found that the percentage of injected embryos displaying the *nat* phenotype is dose dependent. When injected with 9 ng of the MO, 10% of the injected embryos displayed the *nat* phenotype (n = 340). Doubling the concentration (18 ng) resulted in 20% of the injected embryos displaying the *nat* phenotype (n = 165).

fn Expression Is Dynamic during Embryogenesis

The expression pattern of *fn* in zebrafish embryos is complex and dynamic. Maternal message was initially found in a diffuse pattern throughout the blastoderm (data not shown). By the 128-cell stage, the majority of the maternal *fn* message is localized to the marginal blastomeres which participate in the formation of the yolk syncytial layer (YSL) (Figure 4A) (Kimmel and Law, 1985). Zygotic expression of *fn* is initially detected at the onset of gastrulation in the marginal blastomeres (Figure 4B). As gastrulation proceeds, *fn* expression is maintained in the deep layer of the embryo (Figure 4C). Expression analyses in embryos lacking endoderm suggest that this expression pattern is mesodermal (data not shown). At the onset of somitogenesis, *fn* expression is observed in the anterior LPM as well as the tailbud (Figure 4D). This anterior LPM expression is maintained until the 10-somite stage (Figure 4E). Between the 11- and 12-somite stages, *fn* expression is observed in a few cells more medially (Figure 4F). At this stage, *fn* expression also appears in the YSL around the yolk extension and is maintained in the tailbud. The anterior expression spans the midline by the 15-somite stage (Figure 4G). The medial expression of *fn* is maintained throughout the stages of myocardial migration to the midline (data not shown). Examining transverse sections shows that at the 10-somite stage, the *fn* expressing cells are localized within the anterior LPM (Figure 4J), while at the 15-somite stage, *fn* is expressed in two layers of cells, as judged by nuclear staining, at the ventral midline (Figure 4K).

To test the identity of the medial *fn*-expressing cells, we examined *fn* expression in *casanova* (*cas*) and *cloche* (*clo*) mutants which lack endodermal (Alexander et al., 1999) and endocardial (Stainier et al., 1995) cells, respectively. At the 15-somite stage, the expression of *fn* in cells medial to the LPM is absent in *cas* and *clo* mutants (Figures 4H and 4I), suggesting that endodermal and endocardial precursors are required for the medial expression of *fn*.

Fn Deposition at the Midline Is Dispensable for Myocardial Migration

To understand the role of Fn in myocardial migration, we examined its localization in the region where myocardial migration occurs. At the start of myocardial migration, Fn is deposited laterally around the basal surface of the anterior LPM tubules. Fn deposition is also seen at the midline between the endoderm and the endocardial precursors (Figures 5A and 5E). The position of the endocardial precursors at the embryonic midline was confirmed by using a transgenic line that expresses GFP under the control of the promoter for the *flk1* gene (Figure 5E; *flk1*::GFP), one of the earliest markers of all endothelium, including the endocardium (Liao et al., 1997). The generation and expression pattern of this transgenic line will be described elsewhere (D. Beis, J. Chen, and D.Y.R.S.,

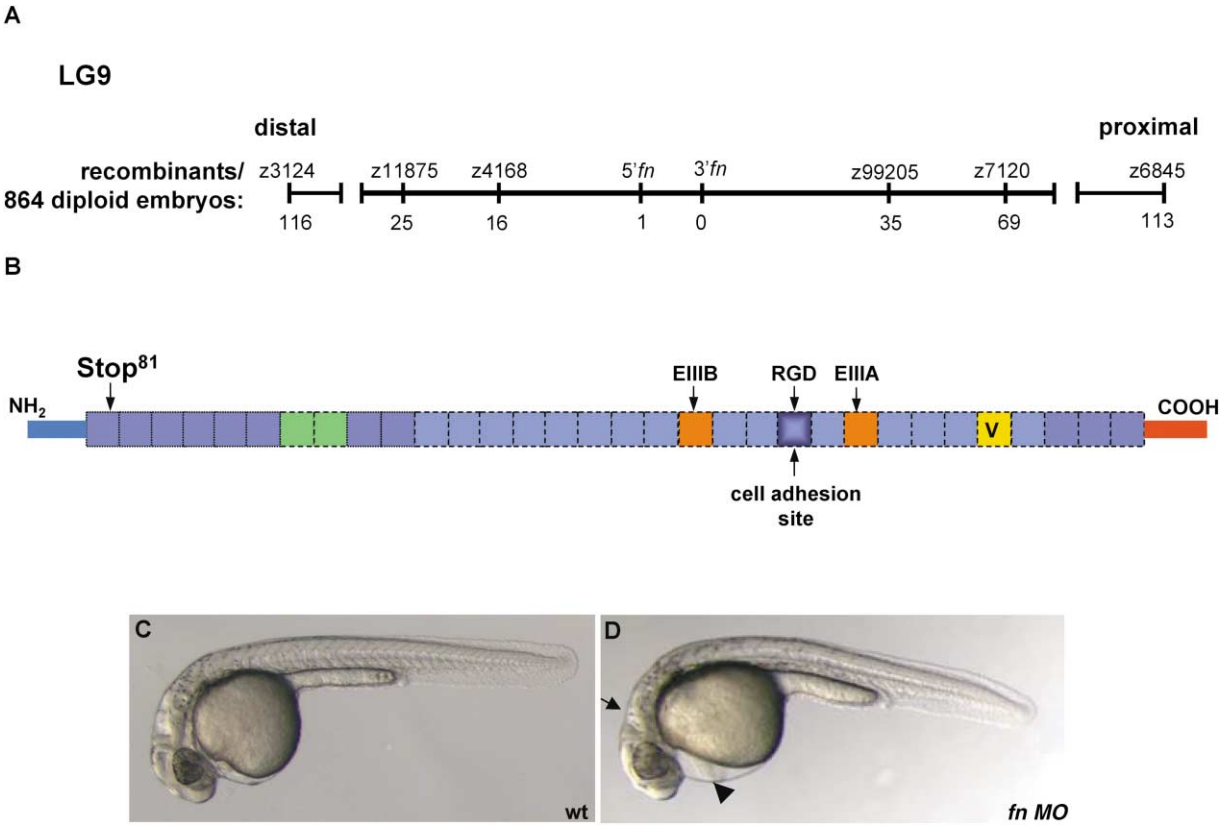

Figure 3. The *nat* Locus Encodes Fn

(A) Genetic map of the *nat* region. Numbers below the CA repeat "z" markers indicate the number of recombination events seen in 864 diploid embryos tested.

(B) Schematic diagram showing the modular structure of Fn. Fn consists of repeating modules of type I (purple), type II (green), and type III (light blue) motifs and alternatively spliced exons (orange) and a variable (V) region (yellow). The *tl43c* mutation introduces a stop codon in the first Fn type I motif (codon 81).

(C and D) Lateral views at 30 hpf, anterior to the left, of wild-type (C) and *fn* MO-injected (D) embryos. MO-injected embryos display pericardial edema (arrowhead) and a flattened hindbrain (arrow) (see Figure 2B for *nat* phenotype).

unpublished data). Fn deposition surrounding the myocardial precursors and between the endoderm and endocardial precursors becomes more prominent as migration proceeds (Figures 5B and 5C).

To examine the consequence of the *nat* mutation on Fn deposition, we analyzed Fn immunoreactivity in *nat* mutants. In *nat* mutants, Fn immunoreactivity was completely absent in the region of the embryo where myocardial migration occurs (Figure 5D). We did occasionally observe staining in the head mesenchyme but at dramatically reduced levels (data not shown), suggesting that some functional Fn may be present in zygotic nat^{tl43c} mutants.

To further characterize the distribution of Fn, we projected confocal sections of wild-type embryos immunostained for Fn. At the 16-somite stage in wild-type embryos, we observed a uniform layer of Fn fibrils spanning the ventral side of the embryo (Figure 5F). As *clo* mutants lack midline *fn* expression prior to myocardial migration (Figure 4I), we also assessed Fn deposition in these mutants. In *clo* mutants, the endocardial precursors are absent (Liao et al., 1997) as confirmed by the lack of *flk1*::GFP expression (Figure 5G). Interestingly, Fn deposition at the midline is also absent, while the myocardial precursors are outlined by Fn deposition (Figure 5G). Projected views of confocal sections of *clo* mutants reveal the complete absence of Fn fibrils at the midline while the laterally Fn deposition around the myocardial precursors appears unaffected (Figure 5H). This result indicates that the midline *fn* expression observed in wild-type embryos (Figure 4G) corresponds to endocardial expression. In addition, this result provided us with an opportunity to assess myocardial migration in the absence of Fn deposition at the midline. At the 20-somite stage when the wild-type myocardial precursors have fused (Figure 5I), *clo* mutants exhibit a delay in myocardial migration and appear similar to 18-somite stage wild-type embryos in which only the posterior myocardial precursors have reached the midline (Figure 5J). However, by 28 hpf, the myocardial precursors in *clo* mutants have reached the midline and formed a dilated linear heart tube (Figure 5L). Thus, an absence of Fn

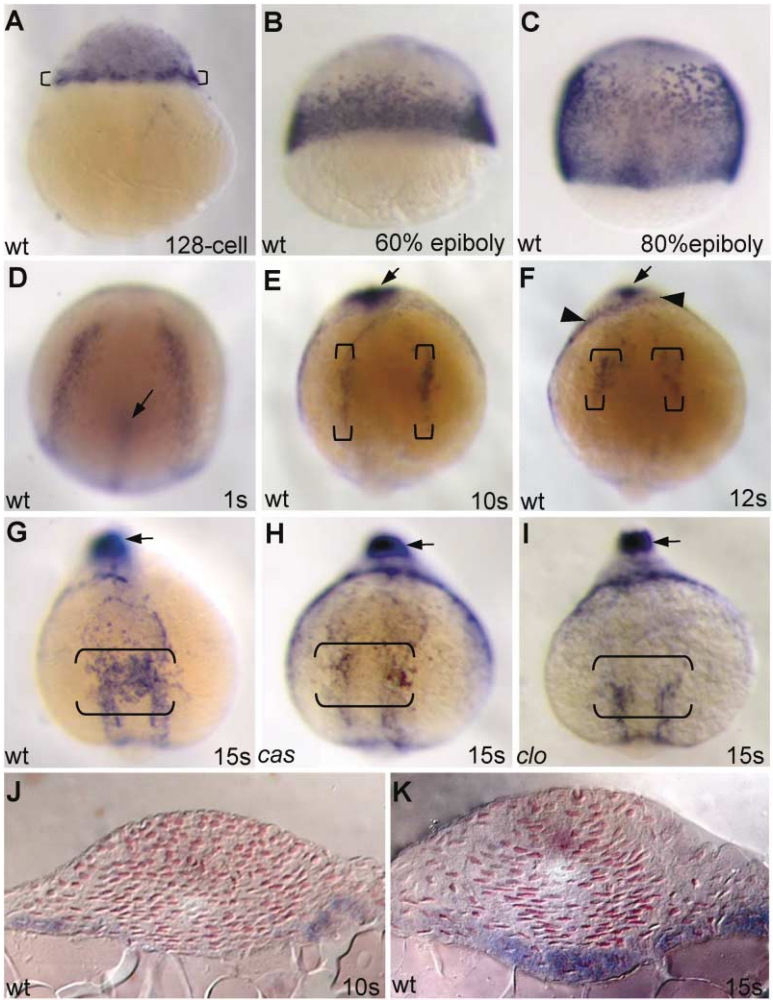

Figure 4. *fn* Expression Is Dynamic during Embryogenesis

(A–G, J, and K) Expression of *fn* in wild-type and (H and I) *cas* and *clo* mutants. (A–C) Lateral views, animal pole to the top; except (C), dorsal view. (D–I) Anteriodorsal views, out-of-focus tailbud to the top. (J and K) Transverse sections, dorsal to the top, counterstained with nuclear fast red.

(A) Maternal message in the 128-cell embryo; the majority of maternal message is localized in the marginal blastomeres (brackets).

(B) At 60% epiboly, *fn* expression is seen in the mesoderm.

(C) At 80% epiboly, *fn* expression is maintained in the mesoderm.

(D) At the 1-somite stage, *fn* expression is seen in the bilateral stripes of the anterior LPM as well as in the tailbud (out of focus; arrow).

(E) At the 10-somite stage, *fn* expression is maintained in the anterior LPM (brackets) and tailbud (arrow).

(F) At the 12-somite stage, *fn* expression becomes patchy in the anterior domain of the embryo (brackets), is maintained in the tailbud (arrow), and also appears in the YSL around the yolk extension (arrowhead).

(G) By the 15-somite stage, expression becomes medially localized, spanning the midline of the embryo (brackets).

(H and I) In *cas* (H) and *clo* (I) mutants, *fn* expression in the medial domain is absent (brackets), while the tailbud expression is unaffected (arrow) at the 15-somite stage.

(J and K) Transverse sections show that at the 10-somite stage, the *fn*-expressing cells correspond to the anterior LPM, while at the 15-somite stage, *fn* is expressed in two layers of cells at the ventral midline.

deposition at the midline is required for the proper temporal regulation of myocardial migration but is dispensable for the migration process.

Fn Deposition Is Required for Junctional Formation and Epithelial Organization in the Migrating Myocardial Precursors

In light of our observations that the myocardial precursors form polarized epithelia and that *nat* mutants exhibit cell adhesion defects, we examined the epithelial organization of the myocardial precursors in *nat* mutants. At the 18-somite stage in wild-type embryos, the myocardial epithelia show apicolateral aPKCs and basolateral β-catenin localization (Figures 6A and 6A′). In *nat* mutants, aPKCs staining is absent in some myocardial precursors while aPKCs localization to the ventricular surface of the neural tube appears unaffected. The mutant myocardial epithelia are also further apart and variably disorganized (Figures 6B and 6B′). By the 20-somite stage in wild-type embryos, the myocardial epithelia show distinct apicolateral aPKCs and basolateral β-catenin localization as well as cell shape differences between medial and lateral cells (Figures 6C and 6C′). In *nat* mutants, apicolateral aPKCs localization is still absent from some myocardial precursors while the basolateral localization of β-catenin appears relatively unaffected (Figures 6D and 6D′). Additionally, the cell shape differences between medial and lateral myocardial precursors are no longer apparent. Altogether, these data suggest that cell-substratum adhesion is required for the maturation of the myocardial epithelia.

In addition to aPKCs, we also examined localization of the junctional protein zonula occluden-1 (ZO-1), as well as cortical actin. In mature epithelial cells, phalloidin staining highlights the apical actin-belt at the adherens junctions (reviewed by Mitic and Anderson, 1998). At the 20-somite stage, ZO-1 is localized to the lateral membrane of the myocardial precursors (Figures 6E and 6E′). Although actin shows an overlap with ZO-1 in the lateral membrane, it is also localized along the basal side of the myocardial precursors (Figures 6E and 6E″). In *nat* mutants, ZO-1 staining is absent or strongly reduced in the myocardial precursors, while phalloidin staining appears heightened and is no longer restricted to the basolateral domain (Figures 6F and 6F″). The loss of aPKCs and ZO-1 staining in some myocardial cells in *nat* mutants indicates that Fn deposition is required for proper junctional formation and/or maintenance in

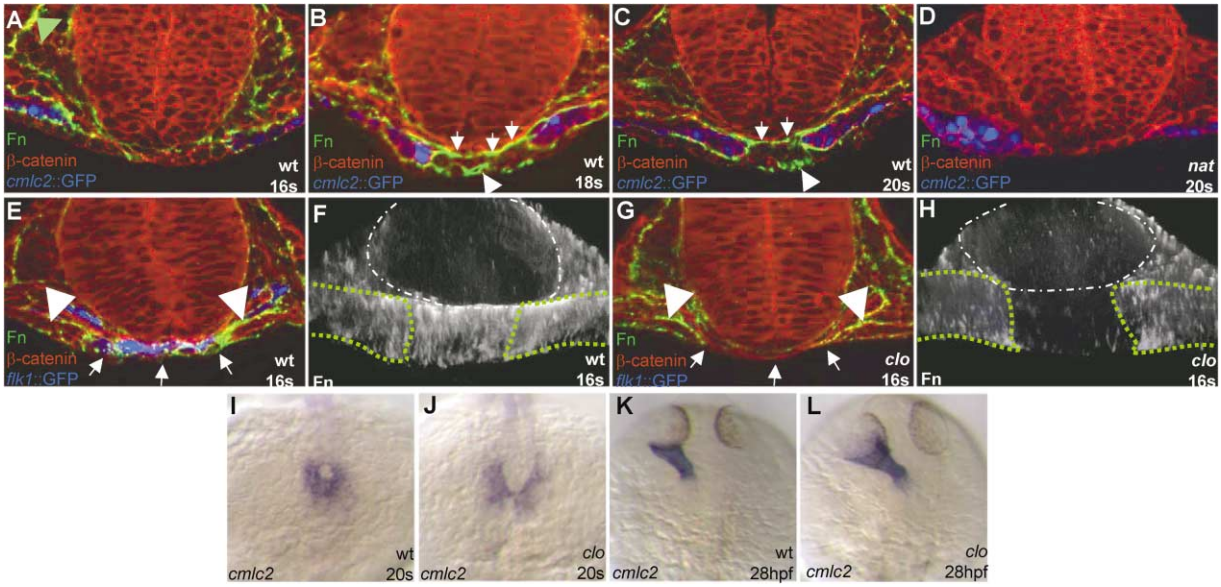

Figure 5. Fn Deposition at the Midline Is Dispensable for Myocardial Migration

(A–D) Transverse sections of *cmlc2*::GFP (false colored blue) and (E and G) *flk1*::GFP (false colored blue) transgenic embryos immunostained for β-catenin (red), Fn (green) in wild-type (A–C, E), *nat* (D), and *clo* (G) mutants at the 16-, 18-, and 20-somite stages; dorsal to the top. (F and H) Projected views of confocal sections collected from (E) and (G) of Fn immunostaining (white), tilted 45° in the Z axis. The positions of the neural tube and myocardial precursors are outlined by white and green dashed lines, respectively. (I–L) *cmlc2* expression in wild-type (I and K) and *clo* mutants (J and L) at the 20-somite and 28 hpf stages.

(A) At the 16-somite stage, Fn is deposited around the myocardial precursors and at the midline between the endoderm and endocardial precursors (blue in [E]). Fn deposition is also seen in the head mesenchyme and lining the basal side of the nonneural ectoderm (green arrowhead).

(B and C) By the 18- and 20-somite stages, Fn deposition appears around the myocardial epithelia, on the ventral side of the anterior endoderm (arrow), and around endocardial precursors (arrowhead).

(D) In *nat* mutants, Fn immunoreactivity is completely absent.

(E) In *flk1*::GFP transgenic embryos, the endocardial precursors (falsed colored blue; arrows) are at the midline between the myocardial precursors that are outlined by Fn immunostaining (green; arrowhead).

(F) Projected view of Fn immunostaining in wild-type embryos shows a uniform layer of Fn fibrils spanning the ventral side of a 16-somite stage embryo.

(G) In *clo* mutants, the endocardial precursors are absent as well as the midline Fn deposition (arrows); however, Fn deposition around the myocardial precursors (arrowhead) appears unaffected.

(H) Projected view of Fn immunostaining in *clo* mutants shows a complete absence of Fn fibrils at the midline.

(I) At the 20-somite stage, wild-type myocardial precursors have fused.

(J) In *clo* mutants, migration of the myocardial precursors is delayed.

(K) In wild-type embryos at 28 hpf, the myocardial precursors have formed a linear tube.

(L) In *clo* mutants by 28 hpf, the myocardial precursors have formed a dilated linear heart tube. The dilation of the *clo* mutant heart is likely due to the lack of endocardial cells. *clo* mutants were presorted based on the absence of *flk1*::GFP expression in the endocardial-endothelial precursors.

the myocardial precursors. This defect in adherens junction formation may account for the adhesion phenotype revealed when examining *cmlc2* expression (Figures 2D and 2E).

Discussion

In this study, we show that the myocardial precursors form polarized epithelia during their movement to the midline, indicating that myocardial cells migrate as coherent populations. From mutant analyses, we show that the zebrafish *nat* gene, which encodes Fn, regulates the morphogenesis of anterior tissues, including that of the myocardial precursors and pharyngeal endoderm. Interestingly, *nat* also appears to regulate myocardial cell-cell adhesion. From mutant analyses, it appears that Fn deposition at the midline is not required for myocardial migration. However, Fn is required for the maturation of the myocardial epithelium, which in turn appears to be critical for its migration.

Epithelial Maturation, Cell-Substratum Adhesion, and Migration

We observed distinct phases in the polarization of the myocardial precursors during their migration to the midline. Initially, the adherens junction proteins aPKCs segregate to the apical membrane and points of cell-cell contacts (Figures 1A and 1D). In mammalian cells, aPKCs are one of the last junctional components recruited to points of cell-cell contact (Suzuki et al., 2002). Thus, the enrichment of aPKCs at the point of cell-cell contacts in the myocardial precursors at the start of

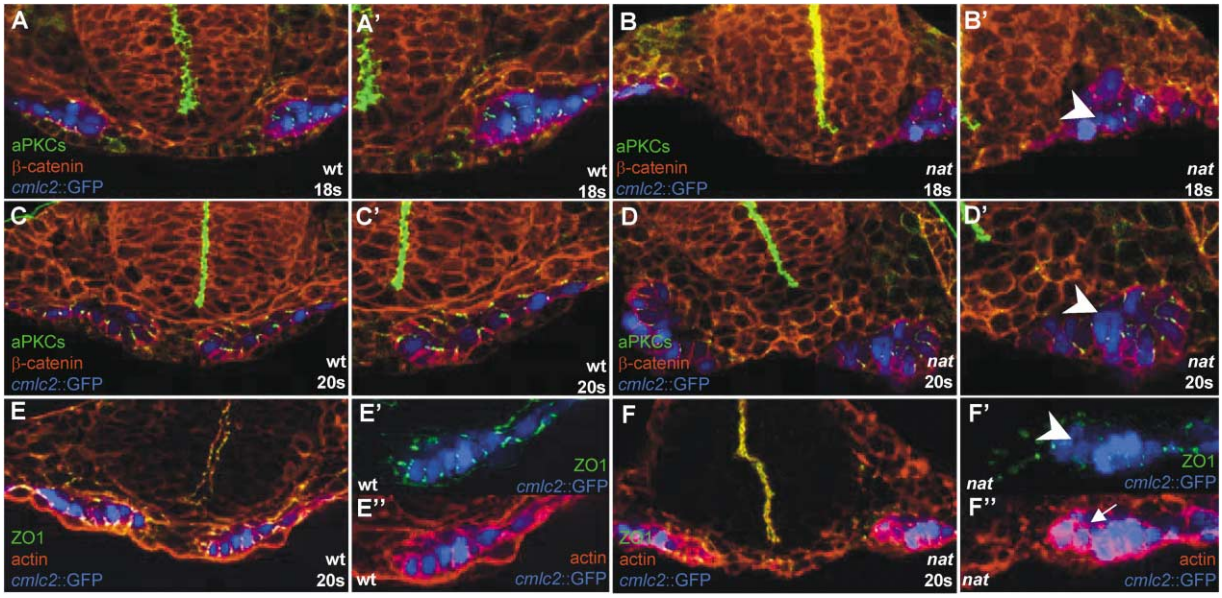

Figure 6. Fn Deposition Is Required for Junctional Formation and Epithelial Organization in the Migrating Myocardial Precursors

Transverse sections of *cmlc2*::GFP (false colored blue) transgenic embryos of wild-type (A, C, and E) and *nat* mutants (B, D, and F) at the 18- and 20-somite stages, immunostained for aPKCs (green) and β-catenin (red) (A–D) or ZO1 (green) and actin (rhodamine-phalloidin) (E and F); dorsal to the top. (A′, B′, C′, D′, E′, E″, F′, F″) Magnified views of the lower right corner of (A)–(F), respectively.

(A and A′) At the 18-somite stage, the myocardial epithelia show apicolateral localization of aPKCs and basolateral localization of β-catenin.

(B and B′) In *nat* mutants, aPKCs staining is absent in some myocardial precursors (arrowhead).

(C and C′) At the 20-somite stage, the medial myocardial precursors are columnar with prominent apicolateral localization of aPKC, while the lateral cells are cuboidal. β-catenin is localized to the basolateral domain.

(D and D′) In *nat* mutants, aPKCs staining is absent from some myocardial precursors (arrowhead), while β-catenin localization appears relatively unaffected. Additionally, the cell shape difference between medial and lateral myocardial precursors is no longer apparent.

(E, E′, and E″) At the 20-somite stage, ZO-1 is localized to the lateral domain of the myocardial epithelia (E′, ZO-1 only), while actin staining is restricted to the basolateral domain (E″, actin only).

(F, F′, and F″) In *nat* mutants, ZO-1 staining is absent (arrowhead) or reduced in the myocardial precursors (F′, ZO-1 only), while actin appears heightened and is no longer restricted to the basolateral domain (arrow) (F″, actin only).

myocardial migration indicates that the myocardial precursors are forming coherent immature epithelia at these stages. As myocardial migration proceeds, aPKCs become restricted to the apical domain of the lateral membranes. This localization occurred concurrently with the segregation of β-catenin to the basolateral membranes (Figure 1G). Similar steps in the maturation of a polarized epithelium have been observed in multicellular epithelial cysts in culture (Wang et al., 1990). Our phenotypic analyses indicate that cell-substratum interactions mediated by Fn regulate epithelial maturation of the myocardial precursors. In *nat* mutants, we observed defects in adherens junction clustering. However, in the basolateral domain, actin localization expanded while β-catenin appeared relatively unaffected. Thus, loss of cell-substratum adhesion does not appear to cause a complete loss of epithelial polarity. In summary, our data suggest that Fn provides a cue important for establishing cellular asymmetry in the migrating myocardial precursors.

At the stages we observed localization of junctional proteins to points of cell-cell contacts, we also observed migratory cell behavior in the medial cells of the myocardial precursors (Figures 1K and 1L). These observations suggest that the myocardial precursors are migrating to the midline as cohesive populations. In addition, we observed actin localization to the basolateral membrane. The lateral distribution of actin appears to colocalize with ZO-1, which is consistent with the localization of the actin-belt at adherens junctions in epithelial cells. The basal distribution of actin has not been reported in mature epithelia and may reflect the migratory behavior of the myocardial cells. Actin polymerizes at sites of cell-substratum interactions forming focal adhesion complexes in migratory cells (reviewed by Huttenlocher et al., 1995). Thus, it will be interesting to investigate whether the basal membranes of the migrating myocardial precursors are sites of focal adhesions.

Recently, Fn has been implicated in branching morphogenesis during salivary gland formation and proposed to be involved in the conversion of cell-cell adhesion to cell-matrix adhesion (Sakai et al., 2003). Specifically, lack of Cadherin colocalization with Fn and RT-PCR data were presented to argue that binding to Fn leads to a local loss of Cadherins at cell-cell junctions. This model appears to be different from our genetic observations that Fn is required for the maturation of epithelial polarity and cell-cell junctions. The apparent discrepancy between these two models of Fn function may be due to differences between branching morphogenesis and epithelial cell migration and suggests that Fn may have tissue-specific regulatory roles within the embryo.

Epithelial Maturation and Differentiation

During the stages of migration, we observed a maturation of the myocardial epithelia that was characterized

by an increase in polarization of cell junctional proteins as well as cell shape changes. The maturation of the myocardial epithelia may be part of the differentiation process as studies of cardia bifida mutants indicate that migration of the myocardial precursors is coupled to differentiation. Mutations in *hand2* and *gata5* result in severe myocardial differentiation defects and cardia bifida (Yelon et al., 2000; Reiter et al., 1999). It is of interest to note that the anterior LPM of *nat* mutants which appears compact and dysmorphic is similar to that of *han* mutants (Yelon et al., 2000). It will be interesting to examine whether the maturation of the myocardial epithelia occurs properly in *hand2* and *gata5* mutants and whether these differentiation genes might also regulate epithelial maturation.

We observed cell shape differences between the medial and lateral cells of the migrating myocardial epithelia. Gene expression studies during the migration stages indicate that the ventricular and atrial precursors are positioned in a medio-lateral pattern (Yelon et al., 1999). The cell shape differences may reflect the differentiation process by which the myocardial precursors segregate into ventricular and atrial cells. In *nat* mutants, while we observed a loss in cell shape differences, the ventricular and atrial cells appear to differentiate normally as assessed by examining chamber-specific antigens (data not shown). This result suggests that in *nat* mutants the cell shape differences and the segregation of ventricular and atrial cells may be uncoupled. However, the cell shape defects observed in *nat* mutants is consistent with our finding that actin is mislocalized in the migrating myocardial precursors (Figures 6F and 6F′). Cell-substratum adhesion mediated by Fn-Integrin interactions has been shown to regulate the actin cytoskeleton leading to changes in cell shape (Bloom et al., 1999). The lack of morphological differences between medial and lateral myocardial precursors in *nat* mutants may result from the defect in actin cytoskeleton rearrangement.

Fn and Gastrulation

Fn has been implicated in the early morphogenesis of a variety of vertebrate embryos. In amphibian embryos, antibody and RGD peptide blocking experiments have implicated Fn in gastrulation movements (Boucaut et al., 1984; Howard et al., 1992; Ramos and DeSimone, 1996). More specifically, the Fn matrix is thought to play a role in the radial intercalation and epiboly movements of cells in the blastocoel roof of *Xenopus* embryos (Marsden and DeSimone, 2001). However, Fn null mouse embryos do not exhibit gastrulation defects (George et al., 1993). We also did not observe any gastrulation defects in *nat* mutants, but found that *fn* is provided maternally, which may be sufficient for cell movements during gastrulation. The *tl43c* allele is temperature sensitive and exhibits a low penetrance of the mutant phenotype at 22°C (see Experimental Procedures). We have taken advantage of the low penetrance at 22°C to raise homozygous *nat* mutant adults. Initial observations of maternal-zygotic *nat* (*MZnat*) mutants suggest that Fn also participates in gastrulation movements in zebrafish (data not shown). Thus, it will be interesting to further characterize these gastrulation defects and determine whether Fn also regulates cell-cell junctions during gastrulation.

Fn and Myocardial Migration

Our phenotypic studies of the *nat* mutant indicate that Fn is required for the morphogenesis of the anterior LPM, myocardial precursors, and anterior endoderm. However, we did observe variation in these phenotypes. One possible explanation for the variation in phenotype is the contribution of maternal *fn*. Two lines of evidence argue against this possibility. First, *MZnat* mutants that gastrulate do not exhibit a more severe myocardial migration defect (Supplemental Figures S1B and S1C [http://www.developmentalcell.com/cgi/content/full/6/3/371/DC1]). Second, we observed differences in the level of disorganization between the two sides of the myocardial epithelia within a single mutant embryo (Figures 5D and 6B). This variation between the two sides of the myocardial epithelia is not due to residual Fn as we did not detect Fn deposition around the myocardial precursors in these embryos (Figure 5D). Thus, additional regulators of myocardial epithelial organization may be modifying the *nat* phenotype. This hypothesis is consistent with observations in mouse where the Fn null phenotype is highly dependent on genetic background (George et al., 1997).

In chick, it has been proposed that a gradient of Fn at the interface between the endoderm and mesoderm provides a directional substrate for myocardial migration (Linask and Lash, 1986). We observed Fn deposition at the midline on the ventral side of the endoderm, which may be providing a substrate for migration. However, by immunohistochemistry we did not detect a difference in the mediolateral distribution of Fn fibrils. Furthermore, the ability of *clo* mutants to undergo medial migration in the absence of Fn deposition at the midline indicates that in zebrafish the myocardial precursors are not migrating toward an increasing concentration of Fn at the midline. Additionally, we have collected data indicating that Fn alone is not sufficient to direct myocardial migration in the absence of endoderm. Specifically, we found that Fn deposition is present at the midline of embryos lacking endoderm, yet myocardial migration does not occur in these embryos (data not shown). These data argue against an instructive role for Fn in myocardial migration to the midline.

We also observed Fn deposition around the myocardial precursors. In the absence of Fn deposition, the myocardial precursors exhibit defects in cell adhesion and epithelial organization. Moreover, in *clo* mutants in which Fn deposition is absent from the midline but unaffected around the myocardial precursors, epithelial organization occurs properly (data not shown, Figure 5G). Similarly, in the absence of endoderm, Fn deposition around the myocardial precursors and epithelial organization of the myocardial precursors are unaffected (data not shown). These data indicate that the epithelial organization defects in *nat* mutants are not due to a secondary effect of lacking midline Fn. It remained possible that in *nat* mutants the endodermal morphogenesis defects might in turn affect myocardial morphogenesis. However, we examined endoderm development in *nat* mutants and found that while it is sometimes defective, the occurrence and severity of this defect did not correlate with the defect in myocardial migration (Figures 2J and 2K). In addition, the occurrence in *nat* mutants of single myocardial cells that have migrated

away from the main myocardial clusters, a phenotype not seen in endoderm-less mutants such as *cas*, argues strongly that this defect in the integrity of the myocardial epithelium is due to a direct effect of Fn on the myocardium. Together, our data indicate that Fn may not simply be a substrate for migration but that it is required for the maturation of the myocardial epithelia. We therefore propose that Fn is required for the organization of the myocardial epithelia, which in turn is required for the migration of this tissue.

Experimental Procedures

Zebrafish Strains

Adult fish and embryos were maintained as described (Westerfield, 1994). We found that the *tl43c* allele (which was obtained from the Tübingen stock center) is temperature sensitive. At 22°C, *tl43c* in a mixed genetic background causes myocardial migration defects in 10% of the mutants. At 28°C, the penetrance increases to 76%, and at 32°C to 100%. We also found that the expressivity of *tl43c* is sensitive to genetic background. Mutant embryos in an inbred Tübingen background exhibit a less severe myocardial migration defect resulting in midline hearts. For all the experiments described in this paper, we used a mixed genetic background and raised all embryos at 32°C.

Genetic Mapping and Genotyping

Genotyping by RFLP of *tl43c* was performed by PCR (primers: 5′-GGATGTGTTATGGACGGACA-3′ and 5′-GCCAGGAAACATTCATC CAC-3′), followed by restriction digest with MseI. In *nat* mutants, a 185 bp PCR product was reduced to fragments of 109 bp and 76 bp by MseI digestion. The PCR conditions were 94°C for 30 s, 58°C for 30 s, and 72°C for 30 s (40 cycles).

Injections of Morpholino Antisense Oligonucleotides

A morpholino oligo designed against zebrafish *fn* (5′-TTTTTTCA CAGGTGCGATTGAACAC-3′) was dissolved in 5 mM HEPES (pH 7.6). Morpholino injections were performed at the one-cell stage at 9 ng or 18 ng per embryo.

In Situ Hybridization

Whole-mount in situ hybridizations (ISH) were performed as described (Alexander et al., 1998). Double *foxA2* and GFP staining in *cmlc2*::GFP transgenic embryos was performed as follows. In brief, embryos were treated with 100 mM glycine (pH 2.2) after ISH to inactivate alkaline phosphatase (AP) and washed with PBS-T (phosphate buffer saline + 0.1% Tween). Anti-GFP antibody (Torrey Pines BioLab; 1:500) was incubated with embryos overnight at 4°C, followed by anti-rabbit-AP conjugated antibody (Jackson Laboratories; 1:3000) incubation overnight at 4°C and detected with INT/BCIP (Roche). A *fn* in situ probe corresponding to the N terminus and the first two Fn type I motifs was cloned into the pGEMT vector (Promega). The antisense probe was generated by linearizing the *p-fn5′* plasmid with SacII, followed by transcription with SP6 polymerase.

Antibodies and Immunohistochemisty

For antibody staining, embryos were fixed overnight at 4°C in 2% PFA. Fixed embryos were embedded in 4% NuSieve GTG low melting agarose and cut into 250 μm sections with a Leica VT1000S vibratome before antibody staining. Antibody staining was performed in PBDT (1% BSA, 1% DMSO, 0.1% Triton X-100 in PBS [pH 7.3]).

We used the following antibodies: rabbit polyclonal anti-Fn (Sigma) at 1:200, mouse IgG_1 anti-β-catenin (Sigma) at 1:500, mouse IgG anti-ZO-1 (Gift from S. Tsukita) at 1:25, and rabbit polyclonal anti-aPKCs at 1:1000 (Horne-Badovinac et al., 2001). Polymerized actin was detected by phalloidin (Molecular Probe) staining (1:50) using a protocol similar to the antibody staining protocol.

Fluorescence images were acquired using a Zeiss LSM5 Pascal confocal microscope.

Acknowledgments

We thank the Tübingen stock center for the *tl43c* allele, Michel Bagnat, Dimitris Beis, Leonard D'Amico, Sally Horne-Badovinac, Benno Jungblut, Elke Ober, and Nick Osborne for comments on the manuscript and helpful discussions. We are grateful to Drs. Huai-Jen Tsai and Dimitris Beis for generously providing the *cmlc2*::GFP and *flk1*::GFP transgenic lines prior to publication. L.A.T. was supported by a NSF fellowship. This work was supported in part by grants from the NIH (NHLBI) and the Packard Foundation to D.Y.R.S.

Received: August 22, 2003
Revised: January 20, 2004
Accepted: January 21, 2004
Published: March 15, 2004

References

Alexander, J., Stainier, D.Y., and Yelon, D. (1998). Screening mosaic F1 females for mutations affecting zebrafish heart induction and patterning. Dev. Genet. *22*, 288–299.

Alexander, J., Rothenberg, M., Henry, G.L., and Stainier, D.Y. (1999). *casanova* plays an early and essential role in endoderm formation in zebrafish. Dev. Biol. *215*, 343–357.

Bloom, L., Ingham, K.C., and Hynes, R.O. (1999). Fn regulates assembly of actin filaments and focal contacts in cultured cells via the heparin-binding site in repeat III_{13}. Mol. Biol. Cell *10*, 1521–1536.

Boucaut, J.C., Darriberre, T., Boulekbache, H., and Thiery, J.P. (1984). Prevention of gastrulation but not neurulation by antibodies to Fibronectin in amphibian embryos. Nature *307*, 364–367.

Chen, J.N., Haffter, P., Odenthal, J., Vogelsang, E., Brand, M., van Eedan, F.J., Furutani- Seike, M., Granato, M., Hammerschmidt, M., Heisenberg, C.P., et al. (1996). Mutations affecting the cardiovascular system and other internal organs in zebrafish. Development *123,* 293–302.

Cox, R.T., Kirkpatrick, C., and Peifer, M. (1996). Armadillo is required for adherens junction assembly, cell polarity, and morphogenesis during *Drosophila* embryogenesis. J. Cell Biol. *134*, 133–148.

Danen, E.H., and Yamada, K.M. (2001). Fn, integrins, and growth control. J. Cell. Physiol. *189*, 1–13.

David, N.B., and Rosa, F.M. (2001). Cell autonomous commitment to an endodermal fate and behaviour by activation of Nodal signalling. Development *128*, 3937–3947.

Drake, C.J., Davis, L.A., Walters, L., and Little, C.D. (1990). Avian vaculogenesis and the distribution of collagens, I, IV, laminin and fn in the heart primorida. J. Exp. Zool. *255*, 309–322.

George, E.L., Georges-Labouesse, E.N., Patel-Kin, R.S., Rayburn, H., and Hynes, R.O. (1993). Defects in mesoderm, neural tube and vascular development in mouse embryos lacking Fn. Development *119*, 1079–1091.

George, E.L., Baldwin, H.S., and Hynes, R.O. (1997). Fns are essential for heart and blood vessel morphogenesis but are dispensable for initial specification of precursor cells. Blood *90*, 3073–3081.

Griffin, K.J., Stoller, J., Gibson, M., Chen, S., Yelon, D., Stainier, D.Y., and Kimelman, D. (2000). A conserved role for H15-related T-box transcription factors in zebrafish and Drosophila heart formation. Dev. Biol. *15*, 235–247.

Horne-Badovinac, S., Lin, D., Waldron, S., Schwarz, M., Mbamalu, G., Pawson, T., Jan, J., Stainier, D.Y.R., and Abdelilah-Seyfried, S. (2001). Positional cloning of *heart and soul* reveals multiple roles for PKCλ in zebrafish organogenesis. Curr. Biol. *11*, 1492–1502.

Howard, J.E., Hirst, E.M., and Smith, J.C. (1992). Are beta 1 integrins involved in Xenopus gastrulation? Mech. Dev. *38*, 109–119.

Huang, C.J., Tu, C.T., Hsiao, C.D., Hsich, F.J., and Tsai, H.J. (2003). Germ-line transmission of a myocardium-specific GFP transgene reveals critical regulatory elements in the cardiac myosin light chain 2 promoter in zebrafish. Dev. Dyn. *228*, 30–40.

Huttenlocher, A., Sandborg, R.R., and Horwitz, A.F. (1995). Adhesion in cell migration. Curr. Opin. Cell Biol. *7*, 697–706.

Hynes, R.O. (1992). Integrins: versatility, modulation, and signaling in cell adhesion. Cell *69*, 11–25.

Kikuchi, Y., Trinh, L.A., Reiter, J.F., Alexander, J., Yelon, D., and Stainier, D.Y.R. (2000). The zebrafish *bonnie and clyde* gene encodes a Mix family homeodomain protein that regulates the generation of endodermal precursors. Genes Dev. *14*, 1279–1289.

Kimmel, C.B., and Law, R.D. (1985). Cell lineage of zebrafish blastomeres. II. Formation of the yolk syncytial layer. Dev. Biol. *108*, 86–93.

Jiang, Y.J., Brand, M., Heisenberg, C.P., Beuchle, D., Furutani-Seike, M., Kelsh, R.N., Warga, R.M., Granato, M., Haffter, P., Hammerschmidt, M., et al. (1996). Mutations affecting neurogenesis and brain morphology in the zebrafish, *Danio rerio*. Development *123*, 205–216.

Liao, W., Bisgrove, B.W., Sawyer, H., Hug, B., Bell, B., Peters, K., Grunwald, D.J., and Stainier, D.Y.R. (1997). The zebrafish gene *cloche* acts upstream of a *flk-1* homologue to regulate endothelial cell differentiation. Development *124*, 381–389.

Linask, K.K. (1992). N-cadherin localization in early heart development and polar expression of Na+,K(+)-ATPase, and integrin during pericardial coelom formation and epithelialization of the differentiating myocardium. Dev. Biol. *151*, 213–224.

Linask, K.K., and Lash, J.W. (1986). Precardiac cell migration: Fn localization at mesoderm-endoderm interface during directional movement. Dev. Biol. *114*, 87–101.

Linask, K.K., and Lash, J.W. (1988). A role for Fn in the migration of avian precardiac cells. I. Dose-dependent effects of fn antibody. Dev. Biol. *129*, 315–323.

Linask, K.K., Knudsen, K.A., and Gui, Y. (1997). N-cadherin-catenin interaction: necessary component of cardiac cell compartmentalization during early vertebrate heart development. Dev. Biol. *185*, 148–164.

Manabe, N., Hirai, S., Imai, F., Nakanishi, H., Takai, Y., and Ohno, S. (2002). Association of ASIP/mPAR-3 with adherens junctions of mouse neuroepithelial cells. Dev. Dyn. *225*, 61–69.

Marsden, M., and DeSimone, D.W. (2001). Regulation of cell polarity, radial intercalation and epiboly in *Xenopus*: novel roles for integrin and fibronectin. Development *128*, 3635–3647.

McFadden, D.G., and Olson, E.N. (2002). Heart development: learning from mistakes. Curr. Opin. Genet. Dev. *12*, 328–335.

Mitic, L.L., and Anderson, J.M. (1998). Molecular architecture of tight junctions. Annu. Rev. Physiol. *60*, 121–142.

Narita, N., Bielinska, M., and Wilson, D.B. (1997). Wildtype endoderm abrogates the ventral developmental defects associated with GATA-4 deficiency in the mouse. Dev. Biol. *189*, 270–274.

Odenthal, J., and Nüsslein-Volhard, C. (1998). *fork head* domain genes in zebrafish. Dev. Genes Evol. *208*, 245–258.

Piepenhagen, P.A., and Nelson, W.J. (1995). Differential expression of cell-cell and cell-substratum adhesion proteins along the kidney nephron. Am. J. Physiol. *269*, C1433–C1449.

Postlethwait, J.H., and Talbot, W.S. (1997). Zebrafish genomics: from mutants to genes. Trends Genet. *13*, 183–190.

Ramos, J.W., and DeSimone, D.W. (1996). *Xenopus* embryonic cell adhesion to Fibronectin: position-specific activation of RGD/synergy site dependent migratory behavior at gastrulation. J. Cell Biol. *134*, 227–240.

Reiter, J.F., Alexander, J., Rodaway, A., Yelon, D., Patient, R., Holder, N., and Stainier, D.Y.R. (1999). *Gata5* is required for the development of the heart and endoderm in zebrafish. Genes Dev. *13*, 2983–2995.

Sakai, T., Larsen, M., and Yamada, K.M. (2003). Fn requirement in branching morphogenesis. Nature *423*, 876–881.

Schier, A.F., Neuhauss, S.C.F., Helde, K.A., Talbot, W.S., and Driever, W. (1997). The *one-eyed pinhead* gene functions in mesoderm and endoderm formation in zebrafish and interacts with no tail. Development *124*, 327–342.

Sechler, J.L., and Schwartzbauer, J.E. (1998). Control of cell cycle progression by fibronectin matrix architecture. J. Biol. Chem. *40*, 25533–25536.

Stainier, D.Y., Lee, R.K., and Fishman, M. (1993). Cardiovascular development in the zebrafish. I. Myocardial fate map and heart tube formation. Development *119*, 31–40.

Stainier, D.Y.R., Weinstein, B.M., Detrich, H.W., Zon, L.I., and Fishman, M.C. (1995). *cloche*, an early acting zebrafish gene, is required by both the endothelial and hematopoietic lineages. Development *121*, 3141–3150.

Stainier, D.Y., Fouquet, B., Chen, J., Warren, K.S., Weinstein, B.M., Meiler, S.E., Mohideen, M.P.K., Neuhauss, S.C.F., Solnica-Krezel, L., Schier, A.F., et al. (1996). Mutations affecting the formation and function of the cardiovascular system in the zebrafish embryo. Development *123*, 285–292.

Suzuki, A., Ishiyama, C., Hashiba, K., Shimizu, M., Ebnet, K., and Ohno, S. (2002). aPKC kinase activity is required for the asymmetric differentiation of the premature junctional complex during epithelial cell polarization. J. Cell Sci. *115*, 3565–3573.

Topczewska, J.M., Topczewski, J., Shostak, A., Kume, T., Solnica-Krezel, L., and Hogan, B.L. (2001). The winged helix transcription factor Foxc1a is essential for somitogenesis in zebrafish. Genes Dev. *15*, 2483–2493.

Walsh, E.C., and Stainier, D.Y.R. (2001). UDP-Glucose Dehydrogenase required for cardiac valve formation in zebrafish. Science *293*, 1670–1673.

Wang, A.Z., Ojakian, G.K., and Nelson, W.J. (1990). Steps in the morphogenesis of a polarized epithelium. I. Uncoupling the roles of cell-cell and cell-substratum contact in establishing plasma membrane polarity in multicellular epithelial (MDCK) cysts. J. Cell Sci. *95*, 137–151.

Westerfield, M. (1994). The Zebrafish Book. (Eugene, OR: University of Oregon Press).

Wiens, D.J. (1996). An alternative model for cell sheet migration on fn during heart formation. J. Theor. Biol. *179*, 33–39.

Yelon, D., Horne, S., and A.and Stainier, D.Y.R. (1999). Restricted expression of cardiac myosin genes reveals regulated aspects of heart tube assembly in zebrafish. Dev. Biol. *214*, 23–37.

Yelon, D., Ticho, B., Halpern, M.E., Ruvinsky, I., Ho, R.K., Silver, L.M., and Stainier, D.Y.R. (2000). The bHLH transcription factor hand2 plays parallel roles in zebrafish heart and pectoral fin development. Development *127*, 2573–2582.

Zhao, Q., Liu, X., and Collodi, P. (2001). Identification and characterization of a novel fn in zebrafish. Exp. Cell Res. *268*, 211–219.